

1 **Antarctic Ice Sheet freshwater discharge drives**
2 **substantial Southern Ocean changes over the 21st**
3 **century**

4 **Tessa Gorte^{1,2}, Nicole Lovenduski^{1,2}, Cara Nisssen^{1,2}, Jan T. M. Lenaerts¹**

5 ¹Department of Atmospheric and Oceanic Sciences, University of Colorado Boulder, Boulder CO, USA
6 ²Institute of Arctic and Alpine Research, University of Colorado Boulder, Boulder CO, USA

7 **Key Points:**

- 8 • We explore impacts of realistic Antarctic Ice Sheet (AIS) freshwater discharge on
9 the Southern Ocean using a state-of-the-art climate model
10 • AIS discharge drives drastic changes in Southern Ocean stratification, winter deep
11 convection, surface and interior temperature, and sea ice
12 • Our results suggest that regional AIS discharge can have far-reaching impacts on
13 the Southern Ocean that can feedback on the climate system

Corresponding author: Tessa Gorte, tessa.gorte@colorado.edu

Abstract

Multidecadal satellite observations indicate that the Antarctic Ice Sheet (AIS) is losing mass at an accelerating rate, which has the potential to impact many aspects of the coupled climate system. While previous studies have demonstrated the importance of AIS freshwater discharge for regional and global climate processes using climate model experiments, many have applied unrealistic freshwater forcing. Here, we explore the potential Southern Ocean impacts of realistic AIS mass loss over the 21st century in the Community Earth System Model version 2 (CESM2) by applying observation-based historical and ice sheet model-based future AIS freshwater forcing. The added freshwater reduces wintertime deep convective area by 72% while retaining 83% more sea ice. Congruent with other studies, we find the increased freshwater discharge extensively impacts local and remote Southern Ocean surface and subsurface temperature and stratification. These results demonstrate the necessity of accounting for AIS mass loss in global climate models for projecting future climate.

1 Introduction

Since the early 1990s, satellite-based observations have shown that the Antarctic Ice Sheet (AIS) is losing mass. The spatial pattern of AIS mass loss is heterogeneous (Rignot et al., 2019), mostly concentrated in the West Antarctic Ice Sheet (WAIS), which drains into the Amundsen and Bellingshausen Seas in the Southern Ocean (SO) (Velicogna & Wahr, 2006). The Ice sheet Mass Balance Inter-comparison Experiment version 2 (IMBIE2; Shepherd et al. (2018)) estimated that, from 1992-2017, the WAIS lost mass at a rate of 94 ± 27 Gt/y, and concluded that this mass loss has been accelerating (Rignot et al., 2019). Several studies using ice sheet models suggest that AIS mass loss will continue to accelerate in the future, as ice shelf thinning, grounding line retreat, and accelerating ice flow are all expected to continue and perhaps intensify with anthropogenic climate change (Pattyn & Morlighem, 2020; Gilbert & Kittel, 2021; Noble et al., 2020).

Apart from rising sea level (DeConto et al., 2021), AIS mass loss will affect many other aspects of the coupled climate system. Observations point to substantial physical changes in SO sea surface height, sea ice, water mass properties, and dense water formation, and a growing body of work attributes these changes to observed increases in AIS freshwater (FW) discharge (hereafter referred to as AIS discharge) (Jacobs & Giulivi, 2010; Fasullo & Nerem, 2018; Purich & England, 2023; Li et al., 2023). The SO's strong teleconnections to the global climate system mean that regional disruptions can precipitate broader changes elsewhere, across a range of timescales (Cabr e & Gnanadesikan, 2017). Using climate model projections, previous work suggests that AIS FW fluxes will impact the future evolution of global atmospheric temperature and precipitation (Bronse laer et al., 2018), upper ocean stratification (Aiken & England, 2008; Swart & Fyfe, 2013), meridional overturning (Sadai et al., 2020; Moorman et al., 2020), and ocean temperature (Bintanja et al., 2015; Pauling et al., 2016; Park & Latif, 2019).

As AIS mass loss is not yet represented interactively in the latest generation of climate models, the potential impacts of AIS discharge on the coupled climate system are often investigated by directly applying anomalous FW fluxes to the ocean component of a climate model. Several studies apply FW forcing around AIS in a homogeneous fashion (Swart & Fyfe, 2013; Park & Latif, 2019; Purich & England, 2023) – inconsistent with the observed spatial pattern of AIS mass loss. Others aim to capture future melt of the large Ross and Ronne ice shelves, failing to reflect current grounded AIS mass loss (Bintanja et al., 2013, 2015). Pauling et al. (2016) explore potential impacts of spatially heterogeneous FW forcing but, like others (Aiken & England, 2008; Bintanja et al., 2013, 2015), impose FW abruptly with little to no gradual increase. Both Sadai et al. (2020) and Bronse laer et al. (2018) – which slowly increase the FW flux over several decades – employ global climate models (GCMs) from the Coupled Model Intercomparison Project version 5 (CMIP5)

65 and apply a FW forcing based on CMIP5 Representative Concentration Pathway 8.5 (RCP8.5)
66 runoff projections. These past studies have provided foundational understanding of the
67 sensitivity of the climate system to large-scale AIS mass loss, but are unrealistic in rep-
68 resenting the spatio-temporal variability in AIS mass changes and/or do not employ the
69 latest versions of climate models (Landerer & Swenson, 2012).

70 Here, we apply a spatially heterogeneous FW signal that is reflective of the cur-
71 rent spatial pattern of AIS mass loss that increases based on (1) satellite observations
72 for the historical period and (2) CMIP6 Shared Socioeconomic Pathway 5-RCP8.5 (SSP5-
73 8.5) runoff projections for the future period. Furthermore, we leverage the Community
74 Earth System Model version 2 (CESM2), an Earth System Model from the updated suite
75 of models in CMIP6. As we will demonstrate, the modeled Southern Ocean climate sys-
76 tem is highly sensitive to AIS discharge – this discharge drives anomalous trends in ver-
77 tical density stratification and surface and subsurface temperature as well as the seasonal
78 cycles of sea ice and deep convective area. Furthermore, our results indicate that regional
79 AIS discharge can impact these processes across the Southern Ocean basin.

80 2 Methods

81 In this paper, we run two fully coupled climate simulations using CESM2. CESM2
82 is a global climate model operated by the National Center for Atmospheric Research (NCAR),
83 which we ran under historical CMIP6 greenhouse gas forcing from 1970-2015 and SSP5-
84 8.5 greenhouse gas forcing from 2016-2100 with a $\sim 0.9 \times 1.25^\circ$ horizontal resolution (Danabasoglu
85 et al., 2020). The first simulation, CONTROL, runs from 1970-2100 with historical forc-
86 ing through 2015 and SSP5-8.5 atmospheric forcing from 2016-2100. CESM2 preserves
87 mass for the AIS via a mass threshold that, when exceeded, informs the model to trans-
88 port excess mass to the nearest ocean grid cell as solid ice discharge. For our CONTROL
89 simulation, we override this mechanism, and instead point the model to a prescribed runoff
90 value of 2775 Gt y^{-1} ($1 \text{ Gt} = 1 \text{ Gigaton} = 10^{12} \text{ kg}$) which is divided into six drainage
91 basins with spatially variable FW discharge that is constant in time (Figure S1 illustrates
92 the discharge from basal melt and calving assigned to each of the basins derived from
93 Lenaerts et al. (2015)). The second simulation, IMBIE, branches off of the CONTROL
94 simulation in 1992 and is run out to 2100 under the same forcing conditions. In the IM-
95 BIE simulation, AIS FW forcing initially has the same spatial pattern as the CONTROL
96 but is allowed to change in time – we create a more realistic forcing that is observations-
97 based for the historical period (1992-2020) and ice sheet modeling-based for the future
98 period (2021-2100) (Rignot et al., 2019; DeConto & Pollard, 2016). For the observations-
99 based forcing, we apply a linear fit to AIS mass balance data, amalgamated from var-
100 ious products by Rignot et al. (2019) such that FW discharge increases from 2775 in 1992
101 to $\sim 3160 \text{ Gt y}^{-1}$ in 2020 (Figure S1). The future AIS FW forcing is based on output
102 from DeConto et al. (2021) who use a combination of ice sheet and climate modeling to
103 estimate the AIS contribution to global mean sea level out to 2300 under RCP8.5 atmo-
104 spheric warming conditions. Their model output shows steady AIS mass balance through
105 ~ 2050 after which point, the AIS losses mass non-linearly. To reproduce their findings,
106 our IMBIE FW forcing is constant in time from 2021-2050 and increases quasi-exponentially
107 through 2100 ending at a value of 9280 Gt y^{-1} (Figure S1). Our AIS FW regime cor-
108 responds to a total AIS contribution to global mean sea level rise of just over 1 m by 2100.
109 With observations currently indicating that the focus of AIS mass loss is in WAIS, we
110 evenly distribute all of the additional AIS FW flux to the surface coastal grid cells in the
111 co-located drainage basin in the Amundsen and Bellingshausen Seas (AB Seas; 95°W
112 to 145°W) (Figure S1). We also subdivide our FW forcing into its solid (calving) and
113 liquid (basal melt) components. Each basin has its own ratio of solid to liquid FW based
114 on results from Depoorter et al. (2013) and these ratios are held constant for the entirety
115 of the simulations (Figure S1). Over the AIS, calving and basal melt account for $\sim 48\%$
116 and $\sim 52\%$, respectively.

117 For this paper, the SO is defined as the ocean south of 50 °S and we explore up-
 118 per ocean stratification, deep convective area (DCA), surface and interior ocean temper-
 119 ature, and sea ice extent (SIE). We quantify upper ocean stratification as the difference
 120 of the potential density at 200 m and that at the surface ($\Delta\rho_{200\text{-surf}} = \rho_{200} - \rho_{\text{surf}}$)
 121 such that positive numbers correspond to higher densities at depth (i.e. stable stratifi-
 122 cation). DCA is calculated as the combined grid cell area under which the maximum mixed
 123 layer depth exceeds 50% of the bathymetry (Heuzé et al., 2013; Heuzé, 2021). As such,
 124 DCA is purely a metric for how well the water column is mixed. Its existence can be –
 125 but is not necessarily – related to the formation of precursors of Antarctic Bottom Wa-
 126 ter which ultimately depends on the density of the waters involved. CESM2 is one of the
 127 few CMIP6 models that accurately produces deep convection solely in the coastal regions
 128 (Heuzé, 2021). We define the surface ocean as the topmost vertical layer of the ocean
 129 model in CESM2 (10 m thick) and consider anything below the mixed layer ($\sim 100\text{-}150$
 130 m) to be the interior ocean.

131 3 Results

132 4 Results

133 Meltwater changes the density structure of the SO, resulting in enhanced upper ocean
 134 stratification (Figure 1). The SO-averaged difference in stratification, $\Delta\rho_{200\text{-surf}}$, in-
 135 creases for both simulations but significantly more so in the IMBIE simulation (1A). For
 136 the entire 1992-2100 simulation period, the IMBIE simulation $\Delta\rho_{200\text{-surf}}$ increases by
 137 approximately 0.2 kg m^{-3} (44%) while the CONTROL simulation, by comparison, in-
 138 creases by 0.05 kg m^{-3} (16%). The difference in SO stratification between the two sim-
 139 ulations is largely realized in the latter half of the 21st century with much of the increase
 140 in the IMBIE simulation occurring after 2070. The spatial realization of the enhanced
 141 stratification is such that the signal in the IMBIE is largely focused in the AB Seas re-
 142 gion but also present in the Ross and Weddell Seas (Figure 1B-C). In these areas, the
 143 increase in stratification can be upwards of 1 kg m^{-3} which constitutes a first order of
 144 magnitude change on the historical mean state (Figure S1). Whereas, the CONTROL
 145 simulation shows no significant change in stratification over the course of the 21st cen-
 146 tury in these regions. Rather, the CONTROL simulation indicates a small increase in
 147 stratification in the open Southern Ocean, that is also captured in the IMBIE simula-
 148 tion (Figures 1B-C).

149 AIS discharge is associated with a significant reduction in Southern Ocean DCA
 150 (Figure 2). CESM2 develops deep convection in many Antarctic coastal regions in the
 151 historical simulation (Figure 2, yellow regions on map insets). Over the course of the cen-
 152 tury, both the CONTROL and IMBIE simulations project a decline in SO DCA from
 153 June through December, when DCA is at a maximum (Figure 2A). Austral winter DCA
 154 declines by 17% in the CONTROL simulation over the century, driven by anthropogenic
 155 changes other than AIS discharge (e.g., warming). Whereas, in the austral summer when
 156 the DCA is at a minimum, there is no statistically significant change in DCA over time
 157 or between simulations (Figure 2A). Including the effects of AIS discharge leads to a win-
 158 tertime DCA reduction from a median value of 0.34 Mkm^2 to 0.24 Mkm^2 ; $\sim 29\%$ (Fig-
 159 ure 2A). Even with the 29% reduction in wintertime SO DCA in the IMBIE simulation,
 160 the median DCA for every month is within the extrema for the CONTROL (Figure 2A).

161 The AIS discharge-related reduction in SO DCA manifests most strongly in the AB
 162 Seas, where our model simulation projects a 75% decline in DCA in the austral winter
 163 months in the IMBIE simulation. Compared to a 13% decline in DCA for the CONTROL,
 164 this indicates substantially reduced seasonal DCA variability (Figure 2B). By the end
 165 of the century, the medians for the months of May as well as August through Novem-
 166 ber are outside the extremes of the CONTROL DCA. The median CONTROL DCA in
 167 this region is also reduced from August-November but is within the historical DCA dis-

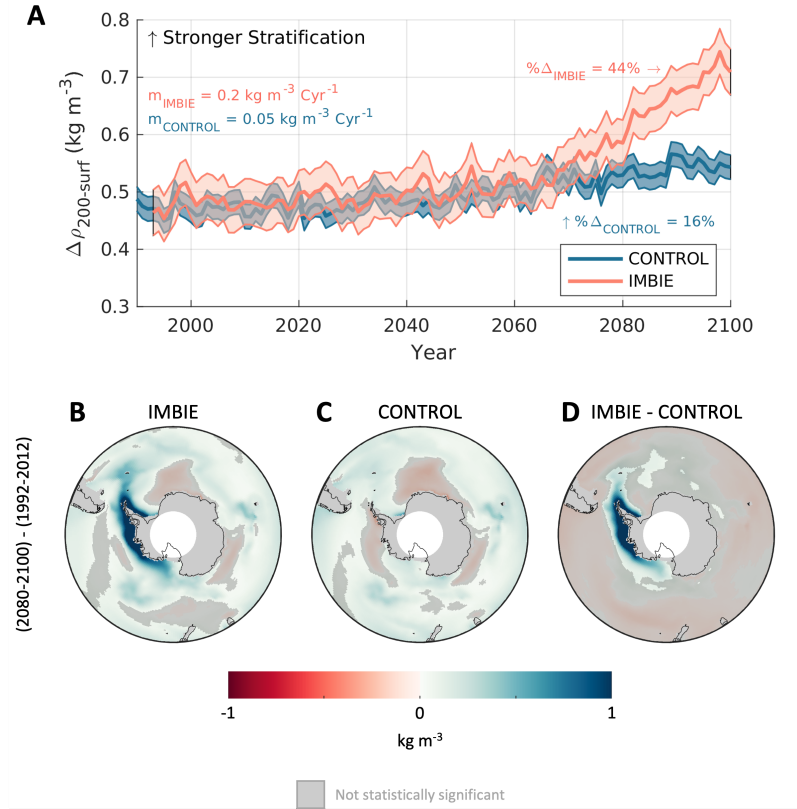


Figure 1. (A) Temporal evolution of the average SO potential density difference between the surface and 200 m depth ($\Delta\rho_{200\text{-surf}}$) over 1990-2100 for both the CONTROL (blue) and IMBIE (peach) simulations. Larger numbers indicate stronger stratification. The solid line shows the SO average for each simulation and the shading indicates 1- σ . (B)-(C) End-of-century (2080-2100) minus beginning-of-century (1992-2012) $\Delta\rho_{200\text{-surf}}$ in the IMBIE and CONTROL simulations, respectively. (D) Map of panel (B) - panel (C) showing the difference in the temporal evolution of stratification between the two simulations. Darker blues indicate stronger stratification with non-statistically significant changes shaded in grey.

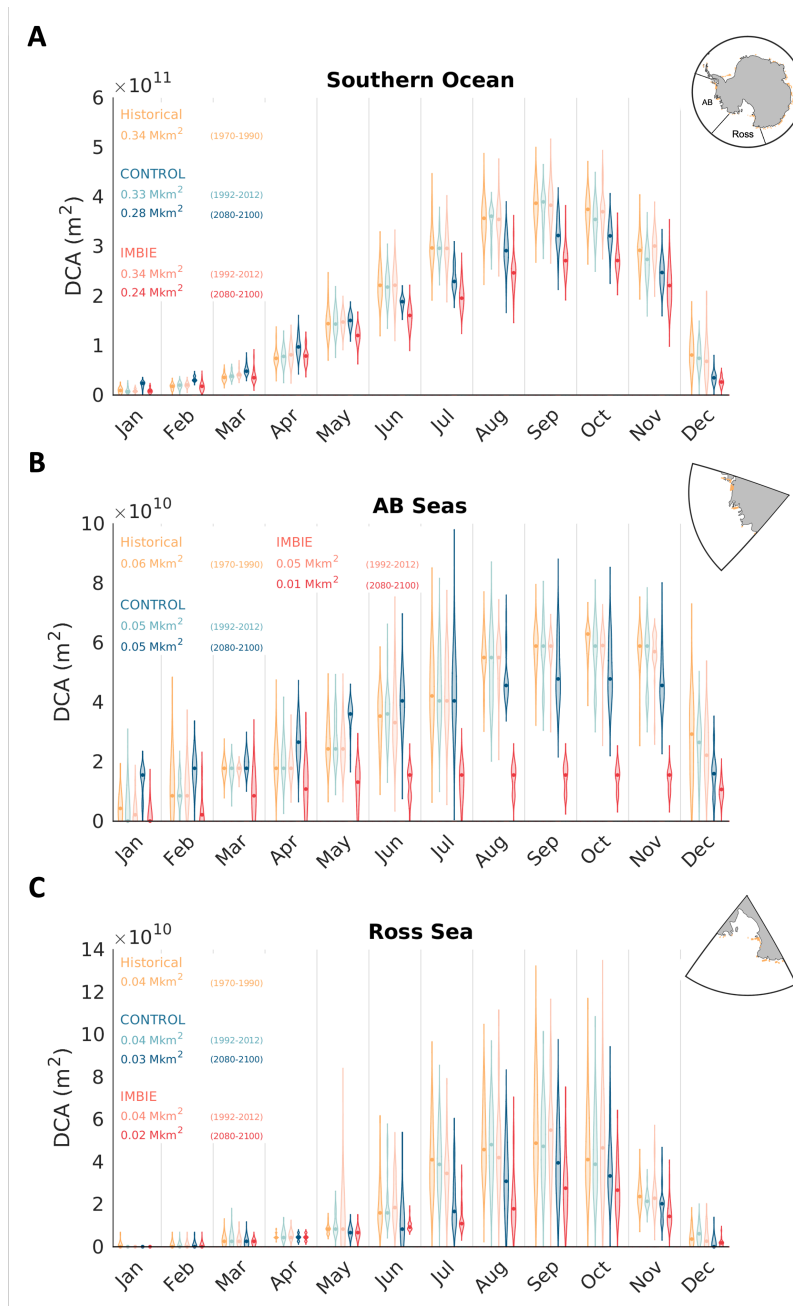


Figure 2. Monthly deep convective area climatology from the (yellow) 1970-1990 historical, (light blue) 1992-2012 CONTROL, (dark blue) 2080-2100 CONTROL, (peach) 1992-2012 IMBIE, and (red) 2080-2100 IMBIE periods/simulations averaged over the (A) Southern Ocean, (B) Amundsen/Bellingshausen Seas, and (C) Ross Sea regions. Maps in the upper right of each panel depict the region of interest as well as the historical DCA (yellow). The violin plots for each month represent the kernel density of DCA distribution. Each violin plot has a dot denoting the median DCA and the ends of the plot extend out to the extrema of the distribution.

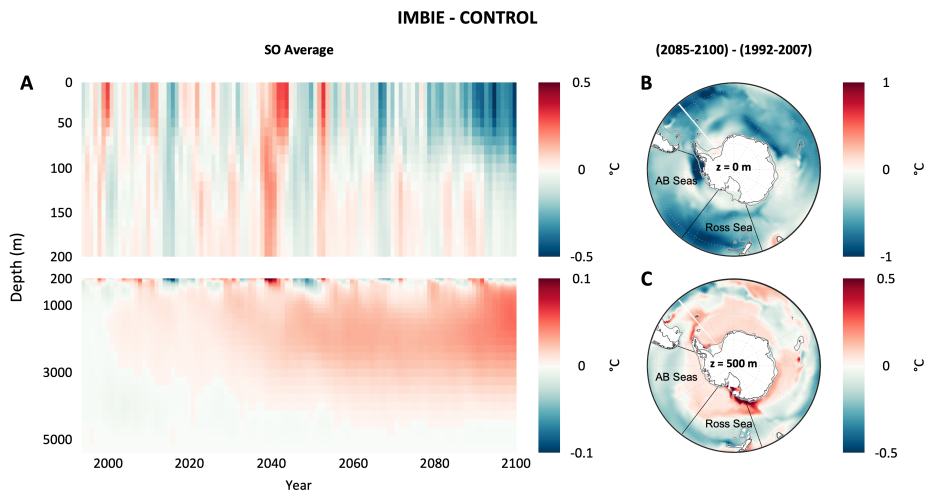


Figure 3. (A) The difference in average SO vertical temperature profile from 1992-2100 between the IMBIE and CONTROL simulations from 1992-2100. The upper panel depicts the top 200 m of the SO and has values ranging from -0.5 to 0.5 $^{\circ}\text{C}$; the lower panel depicts 200 m to the ocean floor with values ranging from -0.1 to 0.1 $^{\circ}\text{C}$. Bluer (redder) colors indicate when and at what depth the IMBIE simulation is cooler (warmer) than the CONTROL. (B) Difference (IMBIE-CONTROL) in SO surface temperature evolution comparing the 2080-2100 period to the 1992-2012 period. (C) Map of the difference (IMBIE-CONTROL) in SO 500 m depth temperature evolution comparing the 2080-2100 period to the 1992-2012 period. Black lines denote the boundaries of the AB Seas and Ross Sea regions.

168 tribution. The Ross Sea, whose DCA historically varies between ~ 0.04 - 0.1 Mkm^2 in the
 169 austral winter and spring shows a 52% reduction in DCA in the IMBIE simulation and a
 170 30% reduction in the CONTROL from July-November. The median IMBIE DCA is
 171 within the broad (and thus highly variable) historical distribution of DCA for the Ross
 172 Sea. As such, our simulations indicate that AIS discharge reduces deep convection both
 173 regionally in the AB Seas as well as in regions outside of where the FW forcing is ap-
 174 plied, such as the Ross Sea.

175 AIS discharge leads to anomalous cooling in the surface and anomalous warming
 176 in the subsurface of the SO. The surface and subsurface SO warm ubiquitously in both
 177 simulations with anthropogenic climate change (Figure S3). The surface SO warms 0.28
 178 $^{\circ}\text{C}$ less in the IMBIE simulation than in the CONTROL by 2100 (1.8 and 1.5 $^{\circ}\text{C}$ respec-
 179 tively). This anomalous cooling, which extends through the mixed layer (~ 100 m), be-
 180 gins to appear mid-century, and intensifies after ~ 2070 (Figure 3A). Anomalous surface
 181 ocean cooling in response to AIS discharge manifests most strongly in the AB Seas re-
 182 gion, where we impose the strongest FW forcing (Figure 3B; Figure S1). Here, surface
 183 temperatures from the IMBIE simulation are nearly 2 $^{\circ}\text{C}$ cooler than those in the CON-
 184 TROL simulation. Another area of anomalous cooling due to FW input manifests off the
 185 coast of the East AIS near Enderby Land; a region of low SIE.

186 In contrast to the surface cooling, the deep SO (500 - 3000 m) experiences anomalous
 187 warming with AIS discharge over the course of the century. Averaged over the SO,
 188 the IMBIE simulation warms by 0.70 $^{\circ}\text{C}$ compared to 0.63 $^{\circ}\text{C}$ in the CONTROL. As such,
 189 the IMBIE simulation is 0.07 $^{\circ}\text{C}$ warmer than the CONTROL on average between 500-
 190 3000 m depth by the end of the century (Figure 3A). The anomalous warming of the

191 deep Southern Ocean is spatially heterogeneous. Figure 3C shows anomalously warm tem-
 192 peratures (~ 0.01 °C) extending from the coast northward to the core of the Antarctic
 193 Circumpolar Current, with much larger anomalies (0.89 °C) in the Ross Sea and along
 194 the Adélie Coast at 500m. Notably, this pocket of anomalously warm water is not co-
 195 located with the AIS FW input.

196 Both simulations show an overall loss of sea ice over the 21st century with anthro-
 197 pogenic climate change, however, the IMBIE simulation shows significantly less exten-
 198 sive sea ice loss, especially in the austral winter/spring (July-November). The histori-
 199 cal SO sea ice cover is largely circumpolar with the highest concentrations in the Wed-
 200 dell and Ross Seas (Figure 4A). By the end of the century (2080-2100) the IMBIE sim-
 201 ulation retains over 50% more sea ice in the AB Seas region (Figure 4B). The Weddell
 202 and Ross Seas – particularly out at the sea ice edge near the peninsula – also preserve
 203 over 25% more sea ice than the CONTROL (Figure 4B). Historical SIE typically reaches
 204 an annual maximum in September-October and an annual minimum between February-
 205 March and can vary between 2-15 Mkm², seasonally, across the entire SO (Figure 4D).
 206 In the AB Seas, SIE varies between 0.25-3.25 Mkm². For both the AB Seas as well as
 207 the entire SO, there is a significant decline in SIE from the 1992-2012 period to the 2080-
 208 2100 period, driven by anthropogenic climate change (Figure 4C-D). However, there is
 209 a significant difference in SIE between the IMBIE and CONTROL simulations by the
 210 end of the century, particularly in the austral winter and spring (Figure 4C-D). For five
 211 months out of the year, the IMBIE simulation produces over 1 Mkm² more total SO sea
 212 ice than the CONTROL in the 2080-2100 period with the maximum, 1.3 Mkm² in Septem-
 213 ber, equivalent to $\sim 9\%$ of the total historical SIE (Figure 4C). This disparity in SIE is
 214 largely due to more sea ice preservation in the AB Seas region, which retains nearly 20%
 215 more sea ice in the IMBIE simulation compared to the CONTROL (Figure 4D).

216 5 Conclusions and Discussion

217 To investigate the potential role of projected AIS discharge on the SO, we conducted
 218 analysis using two fully coupled climate simulations with identical atmospheric forcing
 219 but different AIS FW fluxes. AIS discharge anomalously increases upper ocean strat-
 220 ification by $\sim 30\%$ across the Southern Ocean, with large increases in the AB Seas, and
 221 smaller increases in the Weddell and Ross Seas. End-of century Southern Ocean win-
 222 tertime deep convective area is 0.34 Mkm² in the control simulation, but only 0.24 Mkm²
 223 in the IMBIE simulation. Regionally, we see the strongest impacts in the AB Seas re-
 224 gion as wintertime DCA is reduced to summertime levels while DCA in the Ross Sea de-
 225 clines by $\sim 22\%$ due to the FW. The IMBIE surface ocean is 0.28 °C cooler than that
 226 of the CONTROL while the subsurface warms significantly with warmer regions focused
 227 in the western Ross Sea and along the Adélie Land coast. Our simulations also project
 228 that the freshening and anomalous cooling of the surface SO induce conditions more fa-
 229 vorable for sea ice formation.

230 Our results suggest that the freshening of the AB seas, and to a lesser extent, the
 231 broader Southern Ocean, is the primary driver of the enhanced stratification in the IM-
 232 BIE simulation. Surface temperature cools while subsurface temperature warms in re-
 233 sponse to AIS discharge, a change that would induce reduced stratification if no salin-
 234 ity anomalies were present. The freshening and anomalous cooling of the surface SO in-
 235 duce conditions more favorable for sea ice formation. Previous studies have noted the
 236 importance of the ice-albedo feedback wherein when sea ice melts, it exposes the darker
 237 surface ocean below, lowering the albedo, increasing ocean heat uptake, inducing more
 238 sea ice melt and/or less sea ice growth (Curry et al., 1995). With the IMBIE simu-
 239 lation preserving more sea ice than the CONTROL, this positive feedback loop is suppressed,
 240 and the surface ocean is relatively cooler. When sea ice forms, however, it releases heat
 241 and rejects the oceanic brine, increasing the surface temperature and salinity, and thus
 242 inducing a negative feedback loop. The lower surface temperature and salinity in the IM-

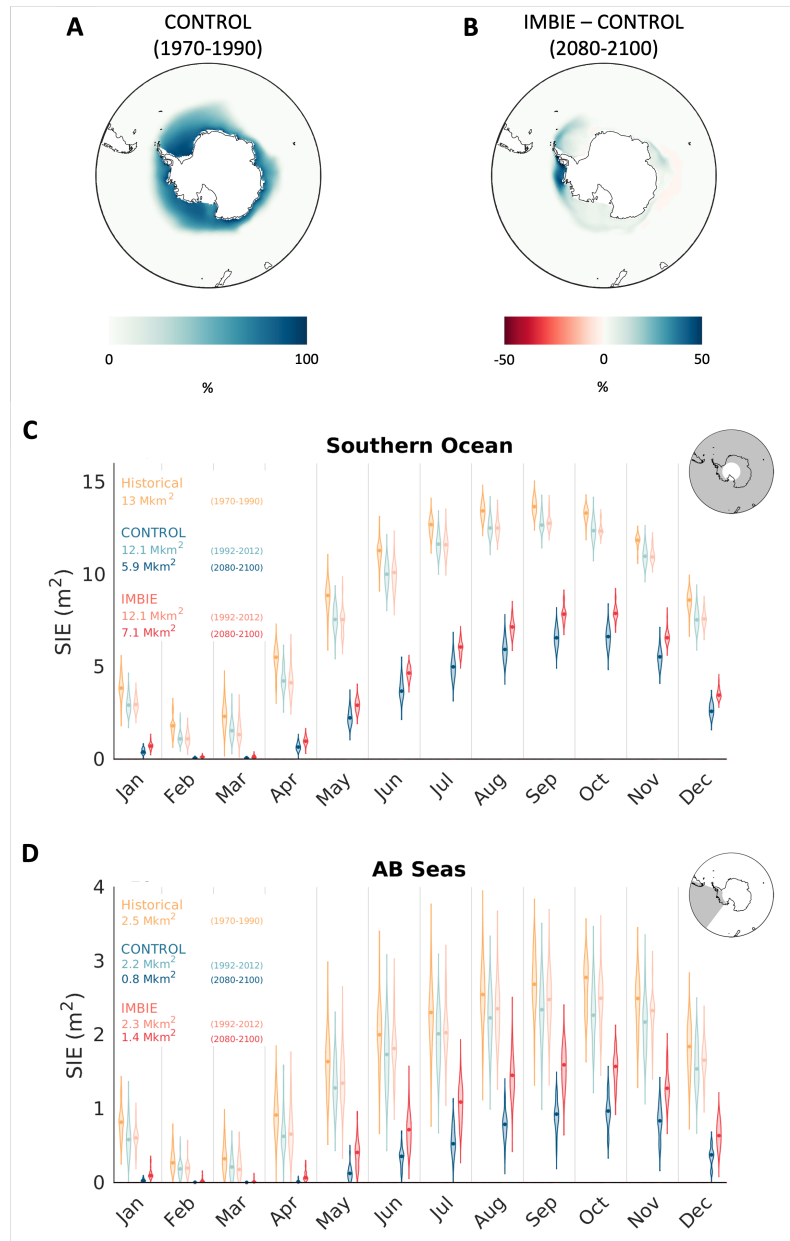


Figure 4. (A) Average annual mean of SIF in each grid cell for the 1970-1990 historical period. (B) the average difference in SIF between the IMBIE and CONTROL simulations during the 2080-2100 period. (C) Monthly SIE for the whole SO in the historical (yellow), 1992-2012 CONTROL (light blue), 2080-2100 CONTROL (dark blue), 1992-2012 IMBIE (peach), and 2080-2100 IMBIE (red) periods. The violin plots for each month represent the kernel density of SIE distribution. Each violin plot has a dot denoting the median SIE and the ends of the plot extend out to the extrema of the distribution.

243 BIE simulation, then, implies that the heat uptake (or lack thereof) and the FW discharge
244 dominate the sea ice formation signal for the evolution of both variables. FW-induced
245 changes to stratification and DCA as well as surface and interior temperature all per-
246 meate into more remote regions of the SO, mainly the Ross and Weddell Seas. Deep con-
247 vection, which only occurs in coastal grid cells, is most strongly affected in the AB Seas
248 but also manifests remotely in the Ross Sea. The loss in DCA is realized predominantly
249 from July-November such that the historical wintertime high is reduced to summertime
250 low levels in the AB Seas. This period aligns with that of the highest sea ice retention
251 – most of the preserved sea ice exists in the AB Seas and, to a lesser extent, the Ross
252 and Weddell Seas.

253 Our findings are supported by those reported in other studies. Compared to Bronselaer
254 et al. (2018), Sadai et al. (2020), and Purich and England (2023), our SIE and surface
255 and interior temperature manifest similarly in strength and spatial pattern with much
256 of the AB Seas sea ice persisting despite strong anthropogenic warming and anomalous
257 warming of the western Ross Sea. We find the sea ice response to be significantly less
258 than what was found in the ice-shelf specific sensitivity experiments of Bintanja et al.
259 (2013) and Bintanja et al. (2015). While we do see a differential sea ice response by the
260 end of the century, the FW-induced changes are not statistically significantly different
261 until after 2070; nearly 80 years into the simulation. As such, we find the minimal sea
262 ice response in extent and trend over <50 model years as seen by Swart and Fyfe (2013)
263 and Pauling et al. (2016), respectively, to be consistent with our results. Bintanja et al.
264 (2013) find that the strength of their FW forcing engenders a sea ice response strong enough
265 to account for the disparate observed SO sea ice cover. Our historical SO sea ice cover,
266 which peaks at $\sim 15 \text{ Mkm}^2$ in September, is already lower than the observed 18-20 Mkm^2
267 in September SIE. Likely owing to anthropogenic warming, there is a significant over-
268 all reduction in SO SIE on the order of $\sim 5\text{-}8 \text{ Mkm}^2$ with the IMBIE simulation retain-
269 ing $\sim 1 \text{ Mkm}^2$ more than the CONTROL by the end of the century. That is to say, the
270 FW discharge does help preserve SO SIE but not enough to offset anthropogenic warm-
271 ing. Like Park and Latif (2019) and Li et al. (2023), we also see a decline in deep con-
272 vection in the SO; both of which use models noted for producing too much open ocean
273 deep convection (Heuzé, 2021).

274 There are three major caveats with this work: (1) the assumption that past obser-
275 vations are a good predictor of future changes, (2) the assumption of ice shelf mass (im)balance,
276 and (3) the application of our FW forcing. We assume that past AIS melt patterns will
277 continue into the future. Our understanding of the decades-to-centuries long spatio-temporal
278 changes to AIS mass balance is limited, as mass change records from the GRACE satel-
279 lite missions are only 20 years long. Ice sheet models – which are informed by these and
280 other observations – project sustained elevated mass loss in the West AIS region over
281 the course of the next century (DeConto & Pollard, 2016). Further, the GRACE satel-
282 lites only measure the mass balance of the grounded ice sheet, not the ice shelves, leav-
283 ing us with little information about large-scale ice shelf mass (im)balances across the AIS.
284 In addition, CESM2 cannot model floating ice shelves. As such, we assume that the AIS
285 ice shelves are in mass balance and that continental mass changes are directly realized
286 as FW fluxes. These FW fluxes, then, are introduced solely to the coastal surface grid
287 cells, though previous work indicates that similar GCMs are sensitive to neither the hor-
288 izontal FW distribution close to or far from the coast nor the vertical FW distribution
289 meaning our FW flux spatial distribution is reasonable for this assessment Bronselaer
290 et al. (2018); Pauling et al. (2016). Finally, we leverage observed AIS mass changes from
291 the GRACE satellites to guide historical (1992-2020) FW discharge and GCM output
292 for future (2021-2100) discharge. The GCM (CESM1) projection we use for future AIS
293 mass balance is (1) based on a model that doesn't have an active ice sheet and, thus, in-
294 herently misses any feedbacks with the coupled climate system and (2) generally con-
295 stant until about 2050, after which point, it increases dramatically (DeConto et al., 2021).

296 Stitching these two forcings together, then, means that from 2021-2050, there is a con-
 297 stant annual FW forcing from the AIS that is guided by limited information.

298 Our results nevertheless demonstrate the potential ramifications of AIS FW dis-
 299 charge on the climate system. AIS FW is likely to play a key role in the spatio-temporal
 300 evolution of the SO over the 21st century. Given the importance of the SO for the up-
 301 take of anthropogenic heat and carbon (Frölicher et al., 2015), it is reasonable to expect
 302 that AIS FW discharge will engender climate feedbacks in the coming century and be-
 303 yond.

304 6 Open Research

305 Data from the CONTROL simulation presented in this paper are publicly avail-
 306 able at <https://doi.org/10.5281/zenodo.8056558> (Gorte et al., 2023a). Data from the IM-
 307 BIE simulation presented in this paper are publicly available at <https://doi.org/10.5281/zenodo.8058223>
 308 (Gorte et al., 2023b).

309 Acknowledgments

310 We would like to thank Dr. Leo van Kampenhout for his work in the setup of these
 311 experiments.

312 This work was performed at the University of Colorado Boulder and Institute of
 313 Arctic and Alpine Research and was supported by the NASA’s Sea Level Change Team
 314 (award #80NSSC20K1123). We would also like to acknowledge NCAR’s Land Ice and
 315 Polar Climate Working Groups for their valuable computing time contributions.

316 References

- 317 Aiken, C. M., & England, M. H. (2008, 8). Sensitivity of the present-day climate
 318 to freshwater forcing associated with antarctic sea ice loss. *Journal of Climate*,
 319 *21*, 3936-3946. doi: 10.1175/2007JCLI1901.1
- 320 Bintanja, R., Oldenborgh, G. J. V., Drijfhout, S. S., Wouters, B., & Katsman,
 321 C. A. (2013, 5). Important role for ocean warming and increased ice-shelf
 322 melt in antarctic sea-ice expansion. *Nature Geoscience*, *6*, 376-379. doi:
 323 10.1038/NNGEO1767
- 324 Bintanja, R., Oldenborgh, G. J. V., & Katsman, C. A. (2015). The effect of in-
 325 creased fresh water from antarctic ice shelves on future trends in antarctic sea
 326 ice. *Annals of Glaciology*, *56*, 120-126. doi: 10.3189/2015AOG69A001
- 327 Bronselaer, B., Winton, M., Griffies, S. M., Hurlin, W. J., Rodgers, K. B.,
 328 Sergienko, O. V., ... Russell, J. L. (2018, 11). Change in future climate
 329 due to antarctic meltwater. *Nature 2018 564:7734*, *564*, 53-58. Retrieved
 330 from <https://www.nature.com/articles/s41586-018-0712-z> doi:
 331 10.1038/s41586-018-0712-z
- 332 Cabré, A., & Gnanadesikan, A. (2017). Global atmospheric teleconnections
 333 and multidecadal climate oscillations driven by southern ocean convec-
 334 tion. Retrieved from www.ametsoc.org/PUBSReuseLicenses doi:
 335 10.1175/JCLI-D-16-0741.s1
- 336 Curry, J. A., Schramm, J. L., & Ebert, E. E. (1995). Sea ice-albedo climate
 337 feedback mechanism. *Journal of Climate*, *8*, 240 - 247. Retrieved from
 338 [https://journals.ametsoc.org/view/journals/clim/8/2/1520-0442](https://journals.ametsoc.org/view/journals/clim/8/2/1520-0442_1995_008_0240_siacfm_2_0_co_2.xml)
 339 [_1995_008_0240_siacfm_2_0_co_2.xml](https://journals.ametsoc.org/view/journals/clim/8/2/1520-0442_1995_008_0240_siacfm_2_0_co_2.xml) doi: [https://doi.org/10.1175/](https://doi.org/10.1175/1520-0442(1995)008(0240:SIACFM)2.0.CO;2)
 340 [1520-0442\(1995\)008\(0240:SIACFM\)2.0.CO;2](https://doi.org/10.1175/1520-0442(1995)008(0240:SIACFM)2.0.CO;2)
- 341 Danabasoglu, G., Lamarque, J. F., Bacmeister, J., Bailey, D. A., DuVivier, A. K.,
 342 Edwards, J., ... Strand, W. G. (2020, 2). The community earth system

- 343 model version 2 (cesm2). *Journal of Advances in Modeling Earth Systems*, *12*,
 344 e2019MS001916. Retrieved from [https://onlinelibrary.wiley.com/doi/](https://onlinelibrary.wiley.com/doi/full/10.1029/2019MS001916)
 345 [full/10.1029/2019MS001916](https://onlinelibrary.wiley.com/doi/abs/10.1029/2019MS001916)[https://agupubs.onlinelibrary.wiley.com/doi/](https://agupubs.onlinelibrary.wiley.com/doi/10.1029/2019MS001916)
 346 [10.1029/2019MS001916](https://agupubs.onlinelibrary.wiley.com/doi/10.1029/2019MS001916) doi: 10.1029/2019MS001916
 347
- 348 DeConto, R. M., & Pollard, D. (2016, 3). Contribution of antarctica to past and fu-
 349 ture sea-level rise. *Nature*, *531*, 591-597. doi: 10.1038/nature17145
- 350 DeConto, R. M., Pollard, D., Alley, R. B., Velicogna, I., Gasson, E., Gomez, N.,
 351 ... Dutton, A. (2021, 5). The paris climate agreement and future sea-
 352 level rise from antarctica. *Nature* *2021 593:7857*, *593*, 83-89. Retrieved
 353 from <https://www.nature.com/articles/s41586-021-03427-0> doi:
 354 10.1038/s41586-021-03427-0
- 355 Depoorter, M. A., Bamber, J. L., Griggs, J. A., Lenaerts, J. T., Ligtenberg, S. R.,
 356 Broeke, M. R. V. D., & Moholdt, G. (2013). Calving fluxes and basal melt
 357 rates of antarctic ice shelves. *Nature*, *502*, 89-92. doi: 10.1038/nature12567
- 358 Fasullo, J. T., & Nerem, R. S. (2018, 12). Altimeter-era emergence of the patterns
 359 of forced sea-level rise in climate models and implications for the future. *Pro-*
 360 *ceedings of the National Academy of Sciences of the United States of America*,
 361 *115*, 12944-12949. doi: 10.1073/pnas.1813233115
- 362 Frölicher, T. L., Sarmiento, J. L., Paynter, D. J., Dunne, J. P., Krasting, J. P., &
 363 Winton, M. (2015). Dominance of the southern ocean in anthropogenic car-
 364 bon and heat uptake in cmip5 models. *Journal of Climate*, *28*, 862-886. doi:
 365 10.1175/JCLI-D-14-00117.1
- 366 Gilbert, E., & Kittel, C. (2021, 4). Surface melt and runoff on antarctic ice shelves
 367 at 1.5°C, 2°C, and 4°C of future warming. *Geophysical Research Letters*, *48*,
 368 e2020GL091733. Retrieved from [https://onlinelibrary.wiley.com/doi/](https://onlinelibrary.wiley.com/doi/full/10.1029/2020GL091733)
 369 [full/10.1029/2020GL091733](https://onlinelibrary.wiley.com/doi/abs/10.1029/2020GL091733)[https://agupubs.onlinelibrary.wiley.com/doi/](https://agupubs.onlinelibrary.wiley.com/doi/10.1029/2020GL091733)
 370 [10.1029/2020GL091733](https://agupubs.onlinelibrary.wiley.com/doi/10.1029/2020GL091733) doi: 10.1029/2020GL091733
 371
- 372 Gorte, T., Lovenduski, N., Nissen, C., & Lenaerts, J. T. (2023a, June). *CESM2*
 373 *CONTROL simulation output: Antarctic Ice Sheet freshwater discharge*
 374 *drives substantial Southern Ocean changes over the 21st century.* Zen-
 375 odo. Retrieved from <https://doi.org/10.5281/zenodo.8056558> doi:
 376 10.5281/zenodo.8056558
- 377 Gorte, T., Lovenduski, N., Nissen, C., & Lenaerts, J. T. (2023b, June). *CESM2*
 378 *IMBIE simulation output: Antarctic Ice Sheet freshwater discharge drives*
 379 *substantial Southern Ocean changes over the 21st century.* Zenodo. Re-
 380 trieved from <https://doi.org/10.5281/zenodo.8058223> doi: 10.5281/
 381 zenodo.8058223
- 382 Heuzé, C. (2021, 1). Antarctic bottom water and north atlantic deep water in cmip6
 383 models. *Ocean Science*, *17*, 59-90. doi: 10.5194/os-17-59-2021
- 384 Heuzé, C., Heywood, K. J., Stevens, D. P., & Ridley, J. K. (2013, 4). Southern
 385 ocean bottom water characteristics in cmip5 models. *Geophysical Research Let-*
 386 *ters*, *40*, 1409-1414. doi: 10.1002/grl.50287
- 387 Jacobs, S. S., & Giulivi, C. F. (2010, 9). Large multidecadal salinity trends near the
 388 pacific-antarctic continental margin. *Journal of Climate*, *23*, 4508-4524. doi:
 389 10.1175/2010JCLI3284.1
- 390 Landerer, F. W., & Swenson, S. C. (2012). Accuracy of scaled grace ter-
 391 restrial water storage estimates. *Water Resources Research*, *48*. doi:
 392 10.1029/2011WR011453
- 393 Lenaerts, J. T. M., Bars, D. L., van Kampenhout, L., Vizcaino, M., Enderlin,
 394 E. M., & van den Broeke, M. R. (2015, 8). Representing greenland ice sheet
 395 freshwater fluxes in climate models. *Geophysical Research Letters*, *42*, 6373-
 396 6381. Retrieved from <http://doi.wiley.com/10.1002/2015GL064738> doi:
 397 10.1002/2015GL064738

- 398 Li, Q., England, M. H., Hogg, A. M., Rintoul, S. R., & Morrison, A. K. (2023, 3).
 399 Abyssal ocean overturning slowdown and warming driven by antarctic melt-
 400 water. *Nature*, *615*, 841-847. Retrieved from [https://www.nature.com/](https://www.nature.com/articles/s41586-023-05762-w)
 401 [articles/s41586-023-05762-w](https://www.nature.com/articles/s41586-023-05762-w) doi: 10.1038/s41586-023-05762-w
- 402 Moorman, R., Morrison, A. K., & Hogg, A. M. C. (2020, 8). Thermal responses to
 403 antarctic ice shelf melt in an eddy-rich global ocean-sea ice model. *Journal of*
 404 *Climate*, *33*, 6599-6620. doi: 10.1175/JCLI-D-19-0846.1
- 405 Noble, T. L., Rohling, E. J., Aitken, A. R., Bostock, H. C., Chase, Z., Gomez, N.,
 406 ... Williams, T. (2020, 12). The sensitivity of the antarctic ice sheet to
 407 a changing climate: Past, present, and future. *Reviews of Geophysics*, *58*,
 408 e2019RG000663. Retrieved from [https://onlinelibrary.wiley.com/doi/](https://onlinelibrary.wiley.com/doi/full/10.1029/2019RG000663)
 409 [full/10.1029/2019RG000663](https://onlinelibrary.wiley.com/doi/full/10.1029/2019RG000663)[https://onlinelibrary.wiley.com/doi/abs/](https://onlinelibrary.wiley.com/doi/abs/10.1029/2019RG000663)
 410 [10.1029/2019RG000663](https://onlinelibrary.wiley.com/doi/abs/10.1029/2019RG000663)[https://agupubs.onlinelibrary.wiley.com/doi/](https://agupubs.onlinelibrary.wiley.com/doi/10.1029/2019RG000663)
 411 [10.1029/2019RG000663](https://agupubs.onlinelibrary.wiley.com/doi/10.1029/2019RG000663) doi: 10.1029/2019RG000663
- 412 Park, W., & Latif, M. (2019, 3). Ensemble global warming simulations with ide-
 413 alized antarctic meltwater input. *Climate Dynamics*, *52*, 3223-3239. doi: 10
 414 .1007/s00382-018-4319-8
- 415 Pattyn, F., & Morlighem, M. (2020, 3). The uncertain future of the antarctic ice
 416 sheet. *Science*, *367*, 1331-1335. Retrieved from [https://www.science.org/](https://www.science.org/doi/10.1126/science.aaz5487)
 417 [doi/10.1126/science.aaz5487](https://www.science.org/doi/10.1126/science.aaz5487) doi: 10.1126/SCIENCE.AAZ5487/
 418 ASSET/D0DE1D3F-7990-45CB-9D79-D9B922FD6075/ASSETS/GRAPHIC/
 419 367_1331_F4.JPEG
- 420 Pauling, A. G., Bitz, C. M., Smith, I. J., & Langhorne, P. J. (2016). The re-
 421 sponse of the southern ocean and antarctic sea ice to freshwater from ice
 422 shelves in an earth system model. *Journal of Climate*, *29*, 1655-1672. doi:
 423 10.1175/JCLI-D-15-0501.1
- 424 Purich, A., & England, M. H. (2023, 1). Projected impacts of antarctic meltwa-
 425 ter anomalies over the twenty-first century. *Journal of Climate*, *36*, 2703-2719.
 426 doi: 10.1175/jcli-d-22-0457.1
- 427 Rignot, E., Mouginot, J., Scheuchl, B., van den Broeke, M., van Wessem, M. J., &
 428 Morlighem, M. (2019). Four decades of antarctic ice sheet mass balance from
 429 1979–2017. *Proceedings of the National Academy of Sciences*, *116*, 1095-1103.
 430 doi: 10.1073/pnas.1812883116
- 431 Sadai, S., Condrón, A., DeConto, R., & Pollard, D. (2020, 9). Future climate re-
 432 sponse to antarctic ice sheet melt caused by anthropogenic warming. *Science*
 433 *Advances*, *6*, eaaz1169. Retrieved from [http://advances.sciencemag.org/](http://advances.sciencemag.org/doi/10.1126/sciadv.aaz1169)
 434 [doi: 10.1126/sciadv.aaz1169](http://advances.sciencemag.org/doi/10.1126/sciadv.aaz1169)
- 435 Shepherd, A., Ivins, E., Rignot, E., Smith, B., Broeke, M. V. D., Velicogna, I., ...
 436 Wouters, B. (2018, 6). *Mass balance of the antarctic ice sheet from 1992 to*
 437 *2017* (Vol. 558). Nature Publishing Group. doi: 10.1038/s41586-018-0179-y
- 438 Swart, N. C., & Fyfe, J. C. (2013, 8). The influence of recent antarctic ice sheet re-
 439 treat on simulated sea ice area trends. *Geophysical Research Letters*, *40*, 4328-
 440 4332. doi: 10.1002/GRL.50820
- 441 Velicogna, I., & Wahr, J. (2006, 3). Measurements of time-variable gravity
 442 show mass loss in antarctica. *Science*, *311*, 1754-1756. Retrieved from
 443 <https://www.science.org/doi/10.1126/science.1123785> doi: 10.1126/
 444 SCIENCE.1123785/ASSET/930F3A74-2360-4753-ADB9-8ED78286A1F8/
 445 ASSETS/GRAPHIC/311_1754_F3.JPEG

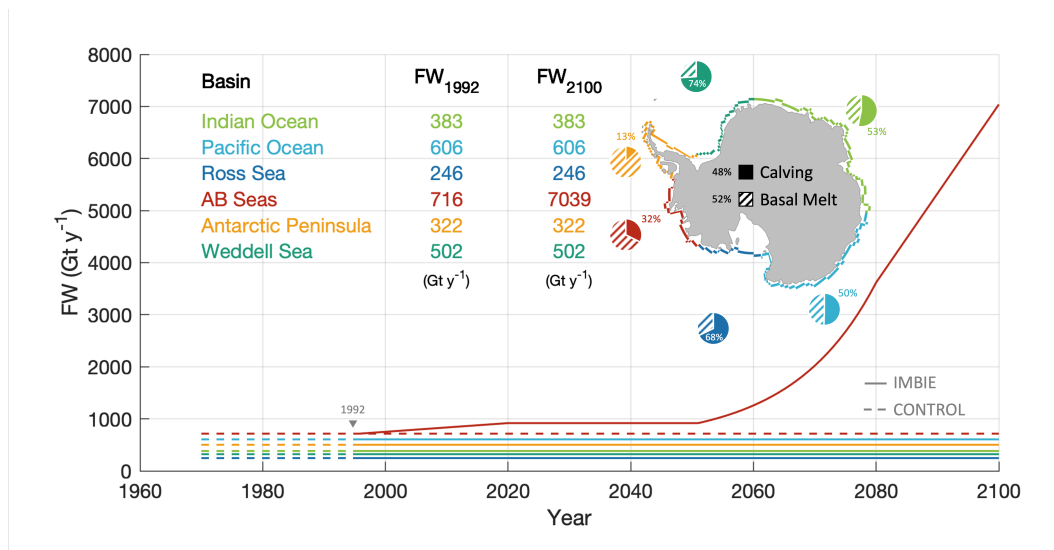


Figure S1. The AIS FW distribution shown spatially and as a time series. The 6 basins we define are the Weddell Sea (dark green), the Indian Ocean (light green), the Pacific Ocean (light blue), the Ross Sea (dark blue), the AB Seas (red), and the Antarctic Peninsula (orange). Each basin has its own ratio of calving to basal melt as depicted by the pie charts (percentages denote the percent of FW flux realized as calving). The time series show the total FW fluxing from each basin for the CONTROL (dashed) and the IMBIE (solid) simulations; the latter of which branches off in 1992. Also displayed are the values of total FW fluxing from each basin in 1992 and in 2100 in Gt y^{-1} .

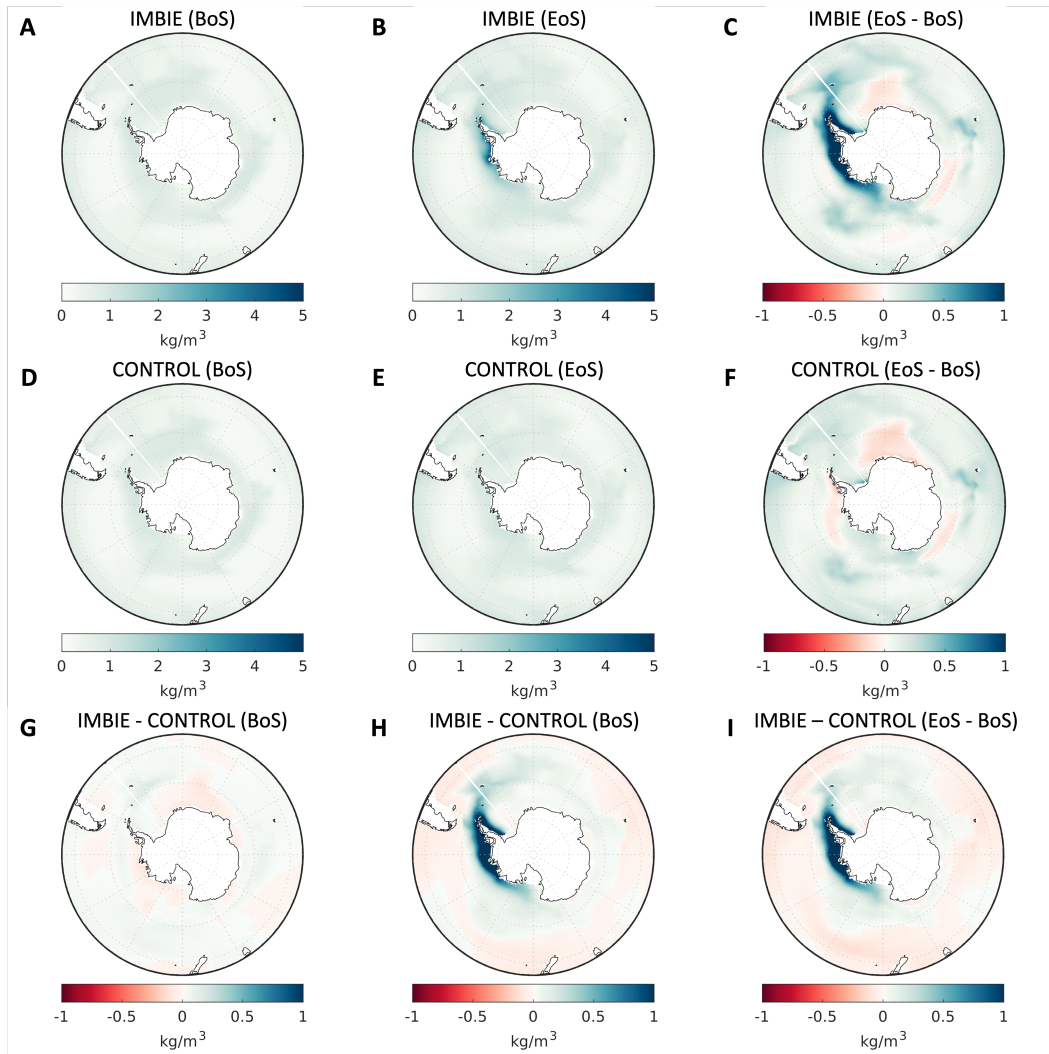


Figure S2. Snapshots of density stratification (200 m - surface) for the IMBIE simulation (top row), CONTROL simulation (middle row), and the difference (IMBIE - CONTROL; bottom row). The columns depict the average stratification for the periods of 1992-2007 (left), 2085-2100 (center), and the difference (right).

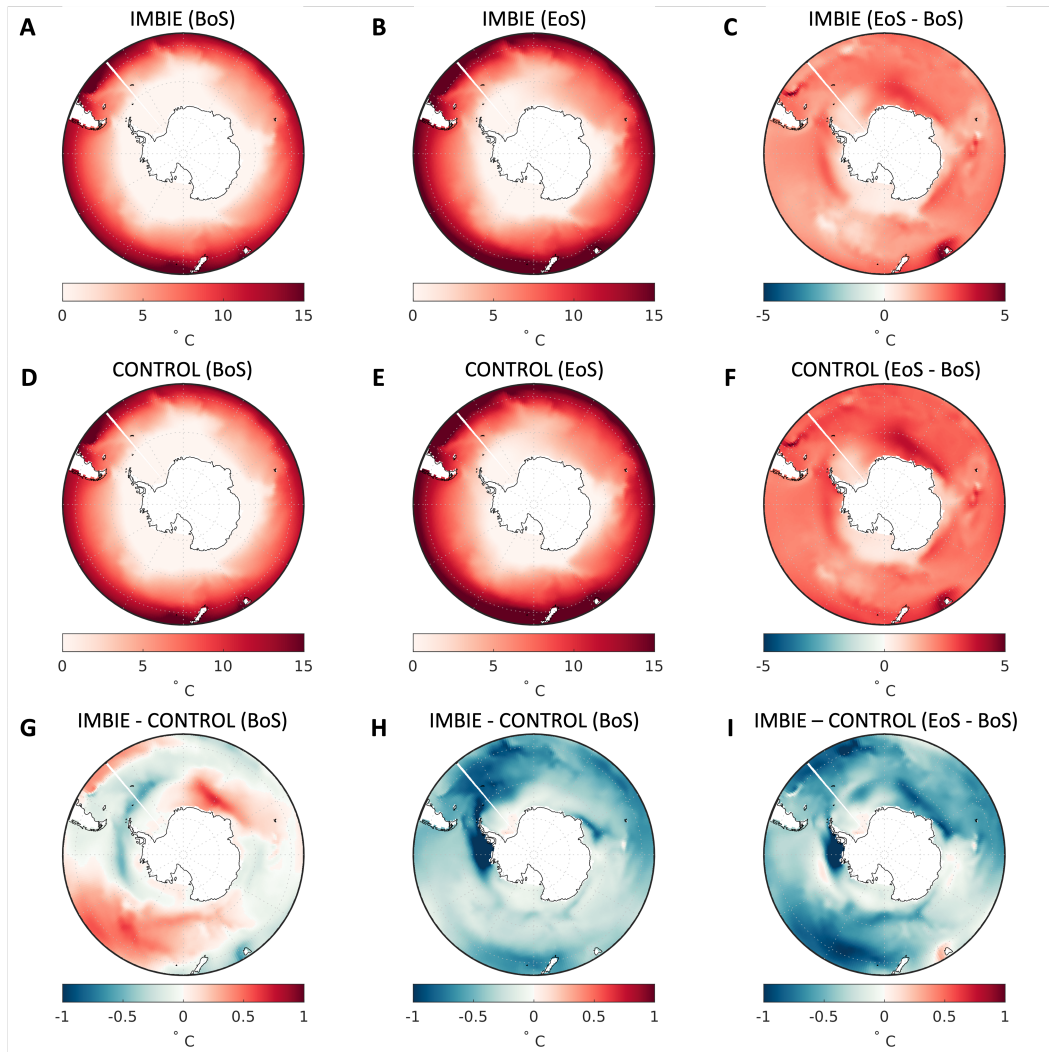


Figure S3. Snapshots of surface temperature for the IMBIE simulation (top row), CONTROL simulation (middle row), and the difference (IMBIE - CONTROL; bottom row). The columns depict the average surface temperature for the beginning of the simulation (BoS) from 1992-2007 (left), the end of the simulation (EoS) 2085-2100 (center), and the difference (right).

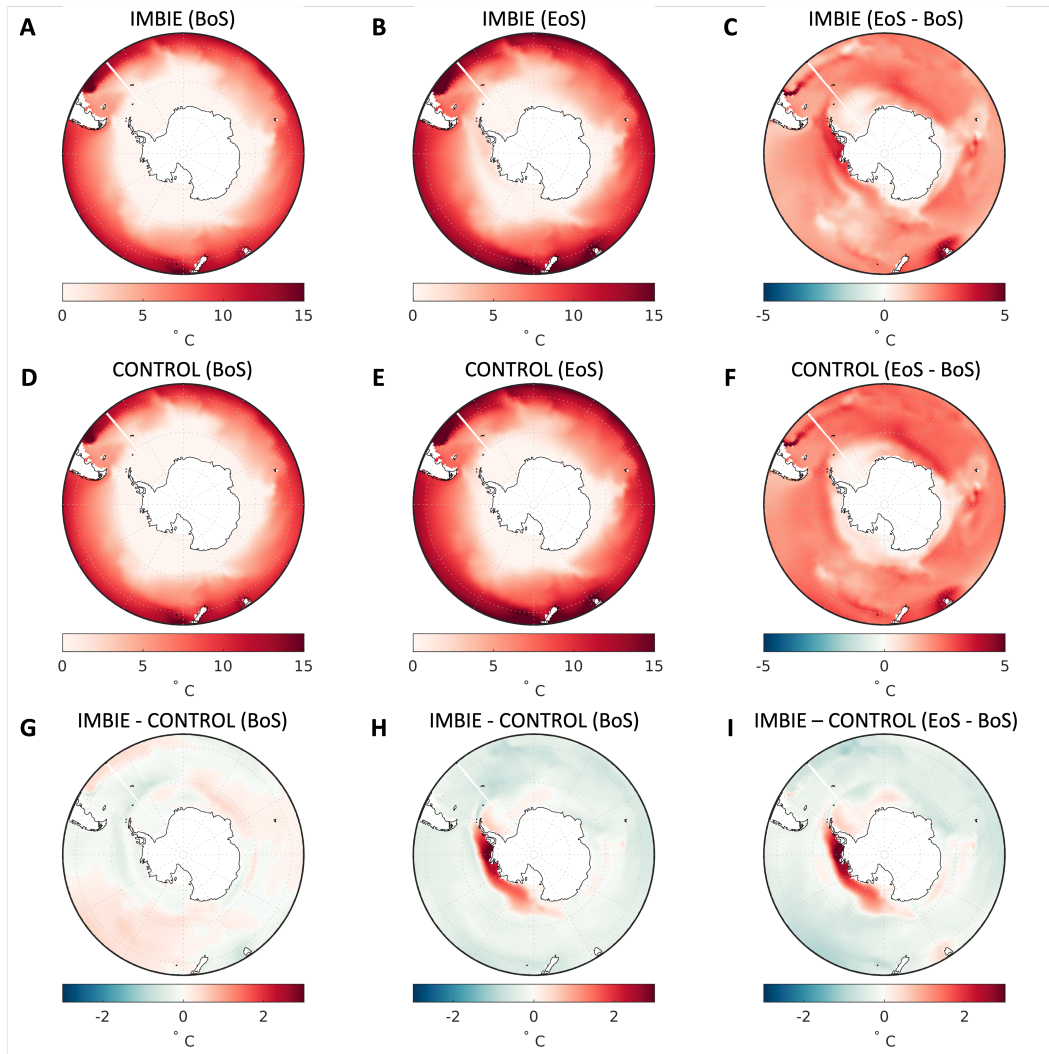


Figure S4. Snapshots of T_{100} for the IMBIE simulation (top row), CONTROL simulation (middle row), and the difference (IMBIE - CONTROL; bottom row). The columns depict the average T_{100} for the beginning of the simulation (BoS) from 1992-2007 (left), the end of the simulation (EoS) 2085-2100 (center), and the difference (right).

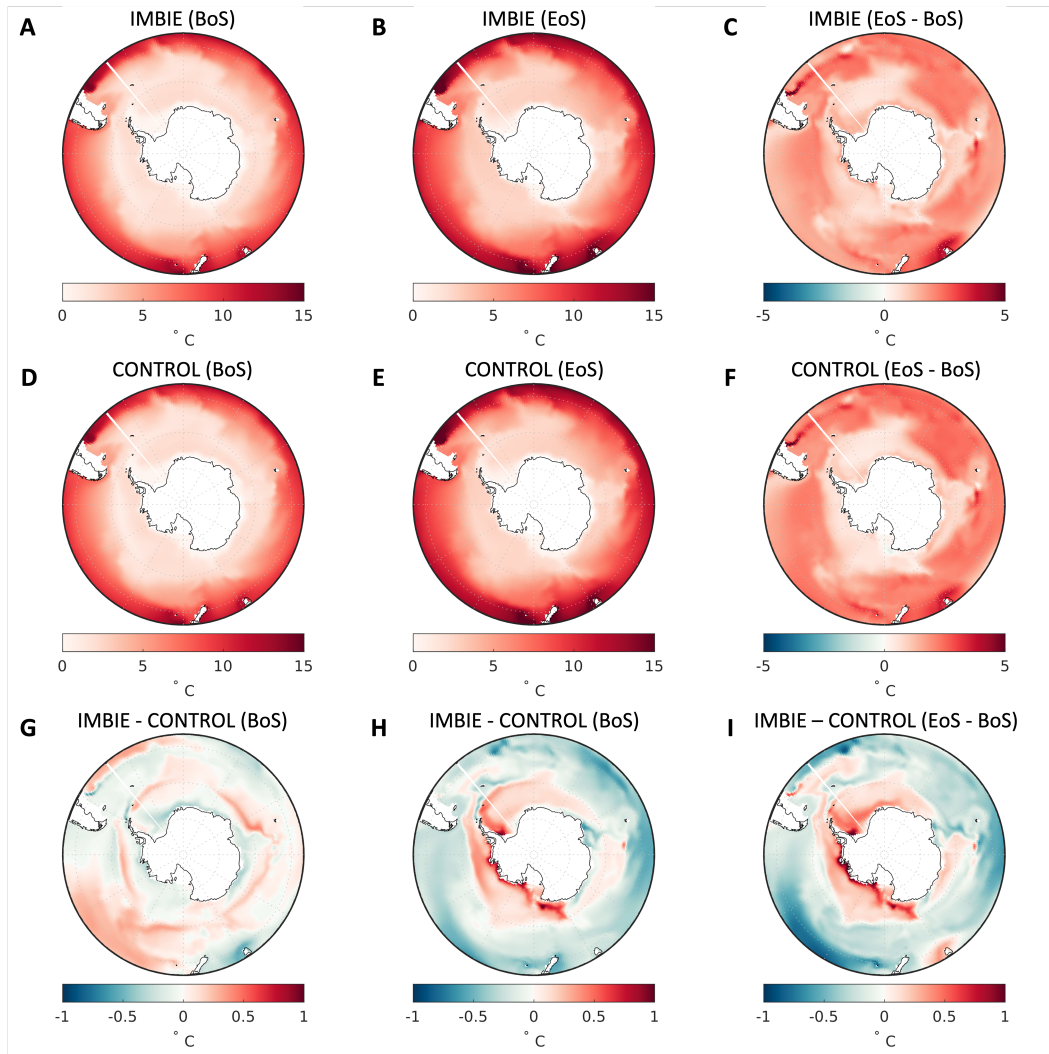


Figure S5. Snapshots of T_{200} for the IMBIE simulation (top row), CONTROL simulation (middle row), and the difference (IMBIE - CONTROL; bottom row). The columns depict the average T_{200} for the beginning of the simulation (BoS) from 1992-2007 (left), the end of the simulation (EoS) 2085-2100 (center), and the difference (right).

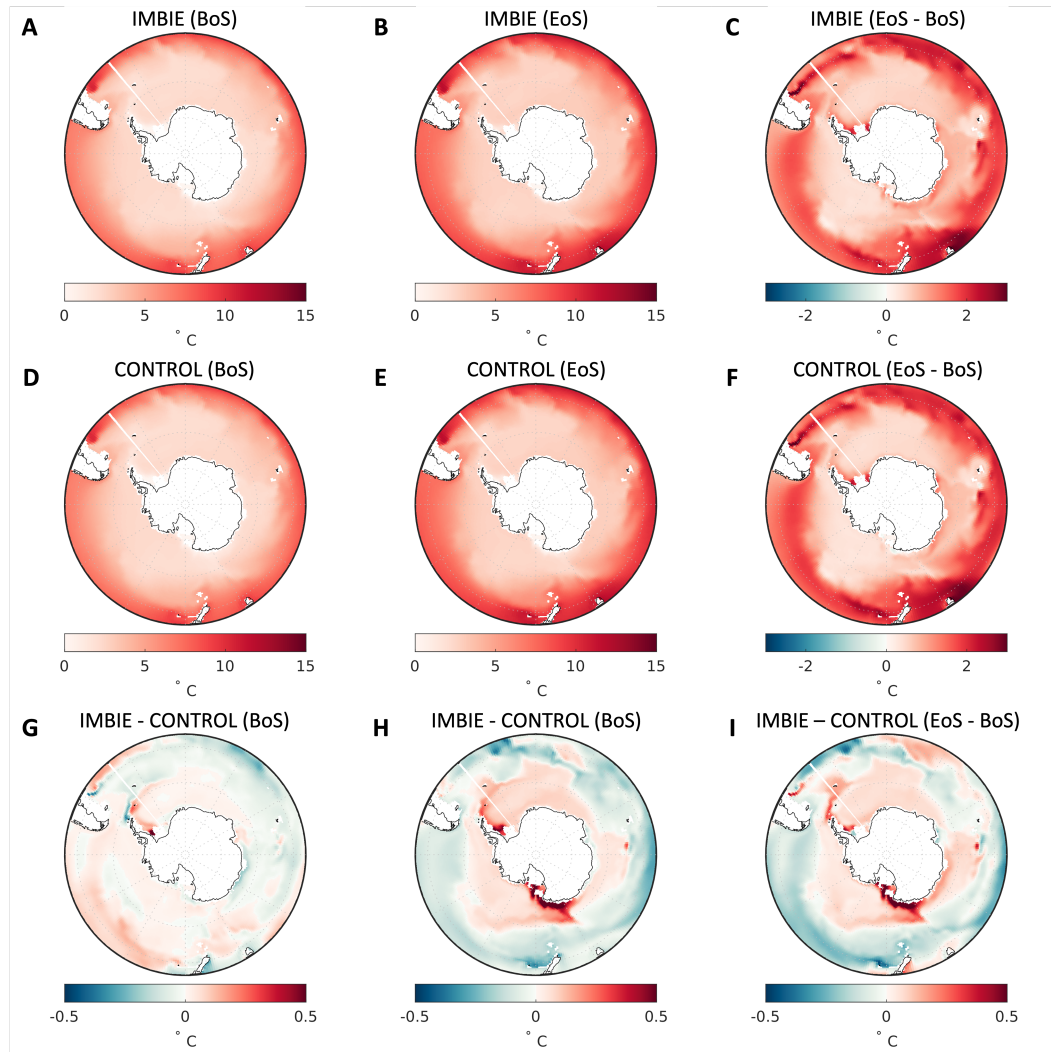
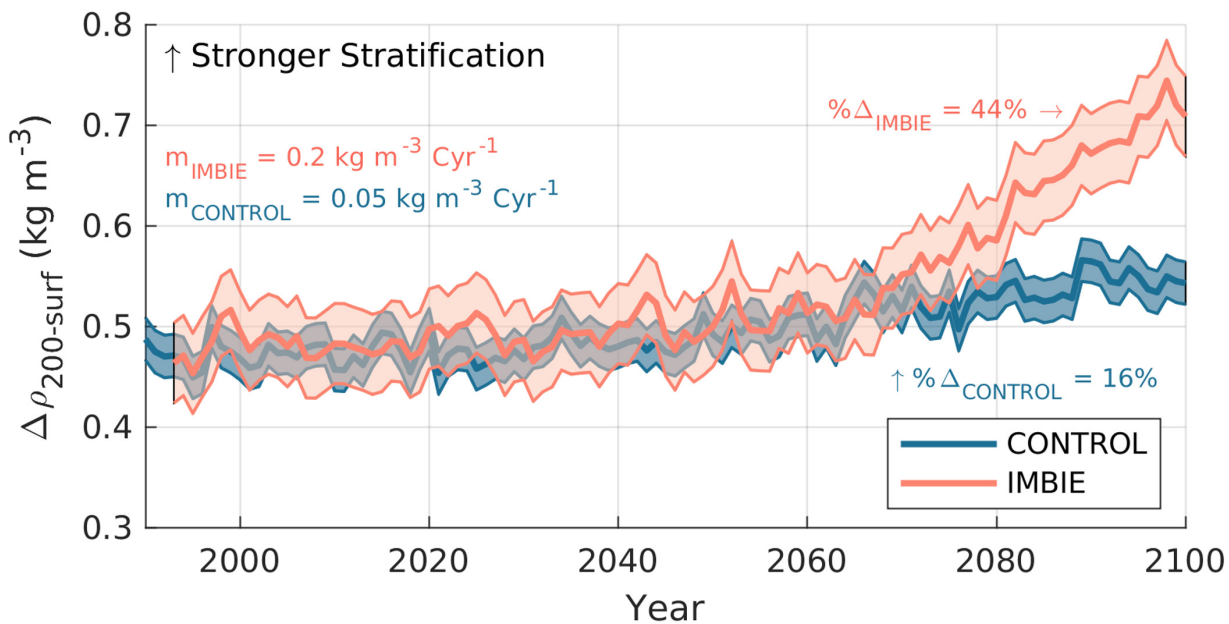
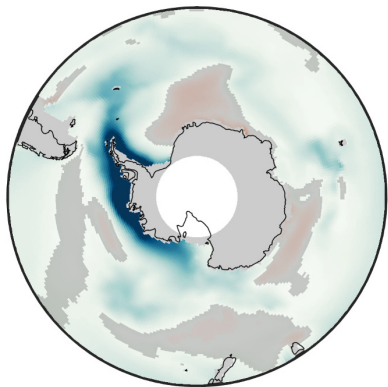


Figure S6. Snapshots of T_{500} for the IMBIE simulation (top row), CONTROL simulation (middle row), and the difference (IMBIE - CONTROL; bottom row). The columns depict the average T_{500} for the beginning of the simulation (BoS) from 1992-2007 (left), the end of the simulation (EoS) 2085-2100 (center), and the difference (right).

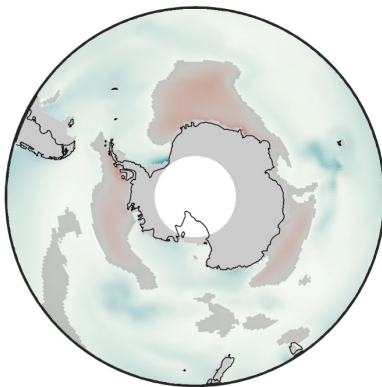
Figure 1.

A**B**

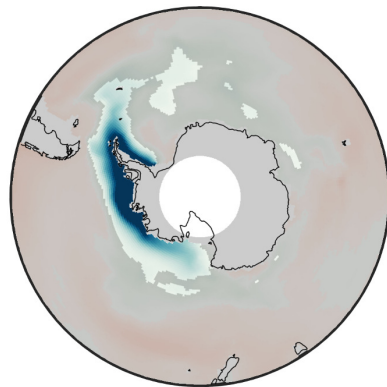
IMBIE

**C**

CONTROL

**D**

IMBIE - CONTROL



-1

0

1

 kg m^{-3} 

Not statistically significant

(2080-2100) - (1992-2012)

Figure 2.

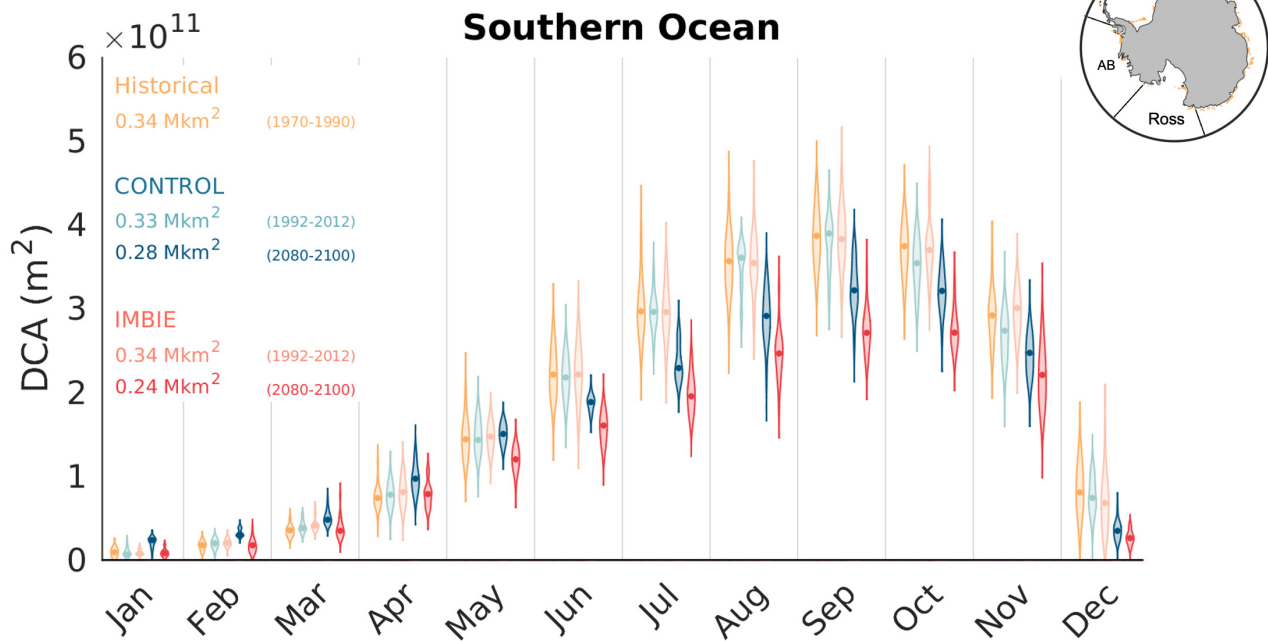
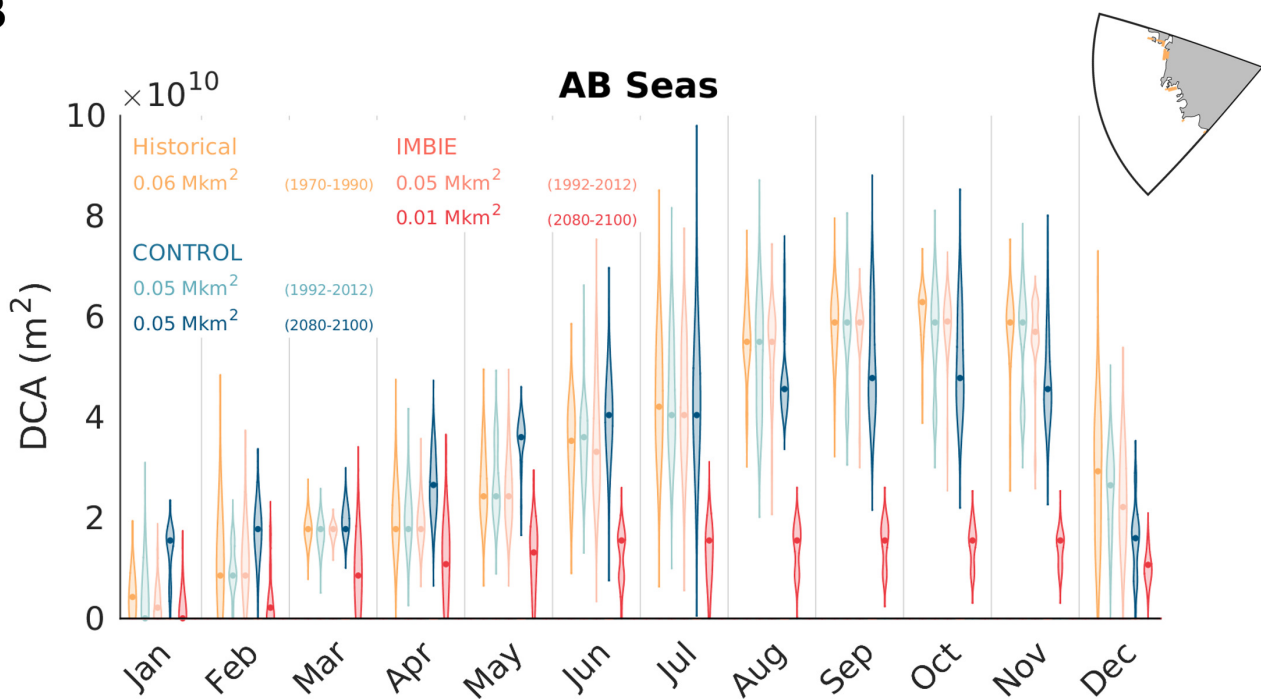
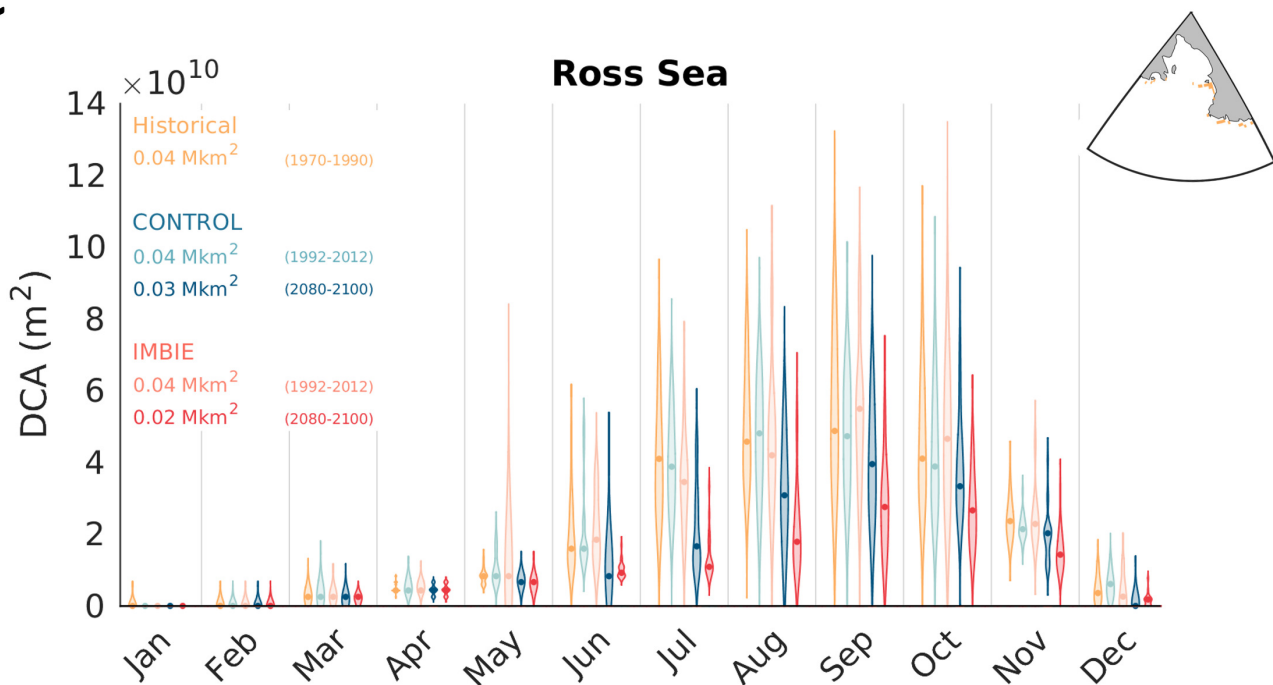
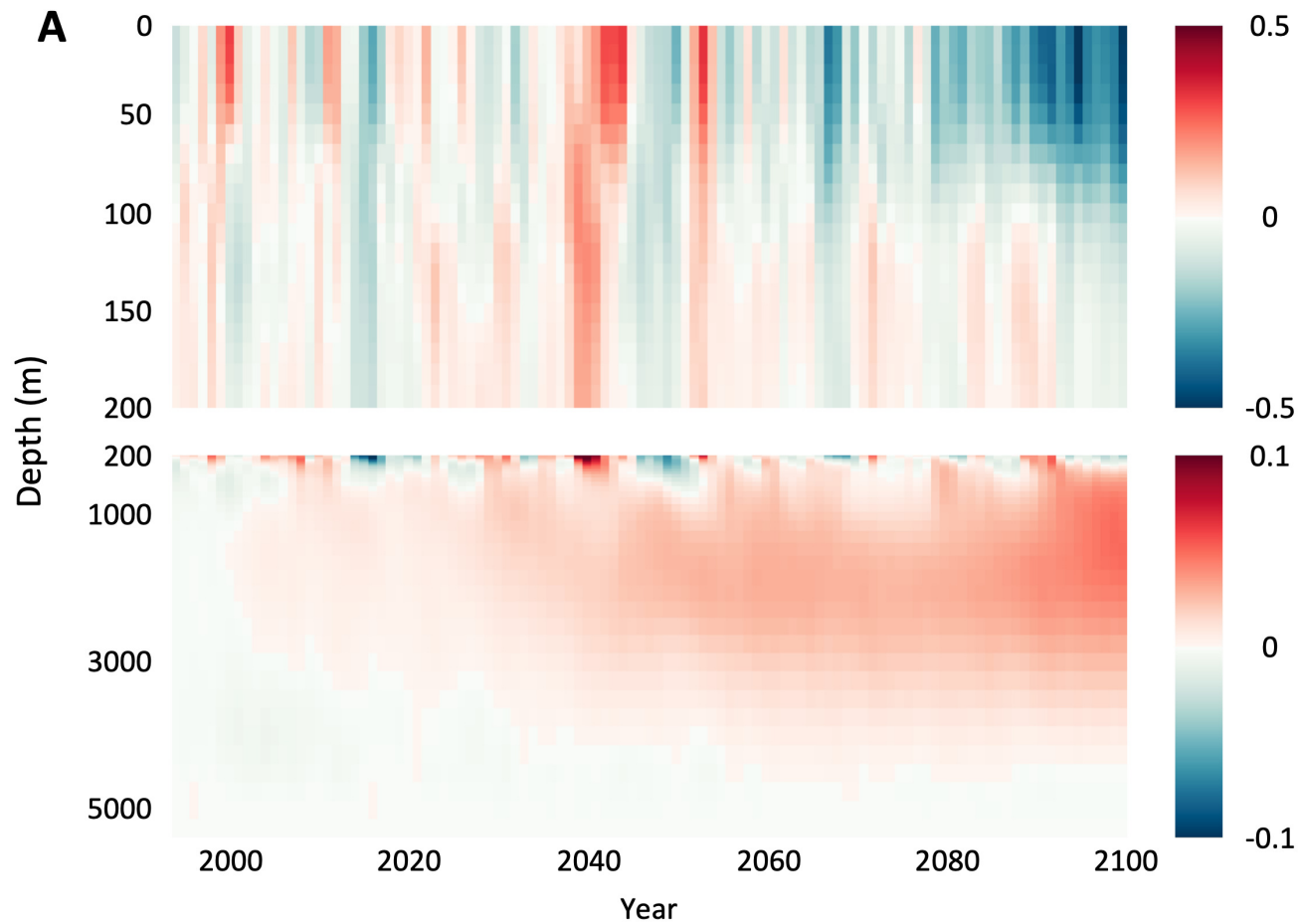
A**B****C**

Figure 3.

IMBIE - CONTROL

SO Average



(2085-2100) - (1992-2007)

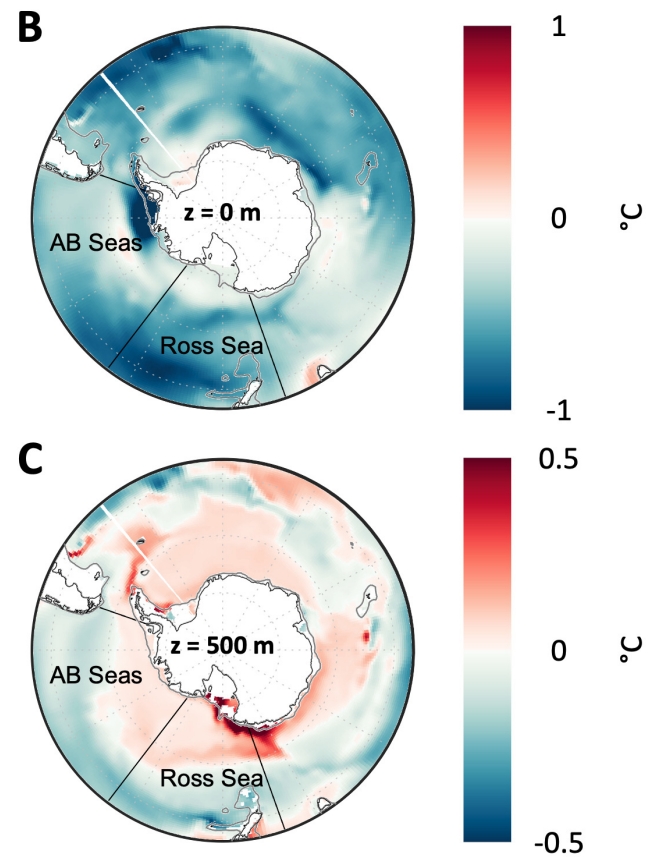
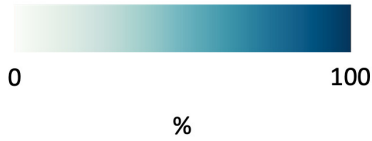
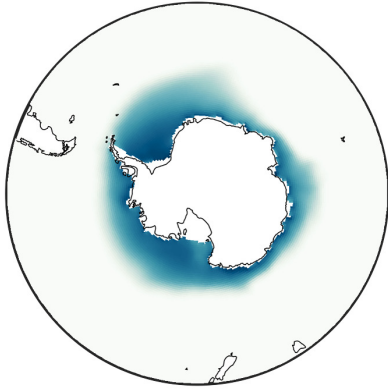
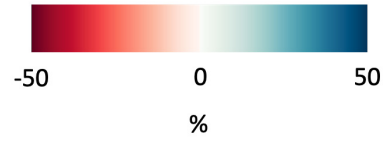
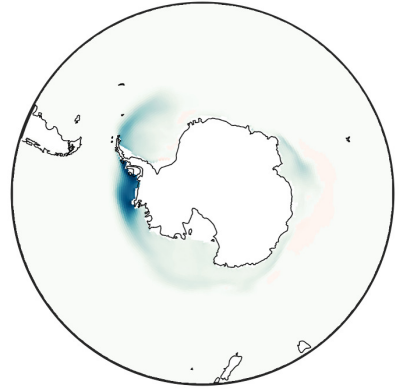


Figure 4.

A CONTROL
(1970-1990)

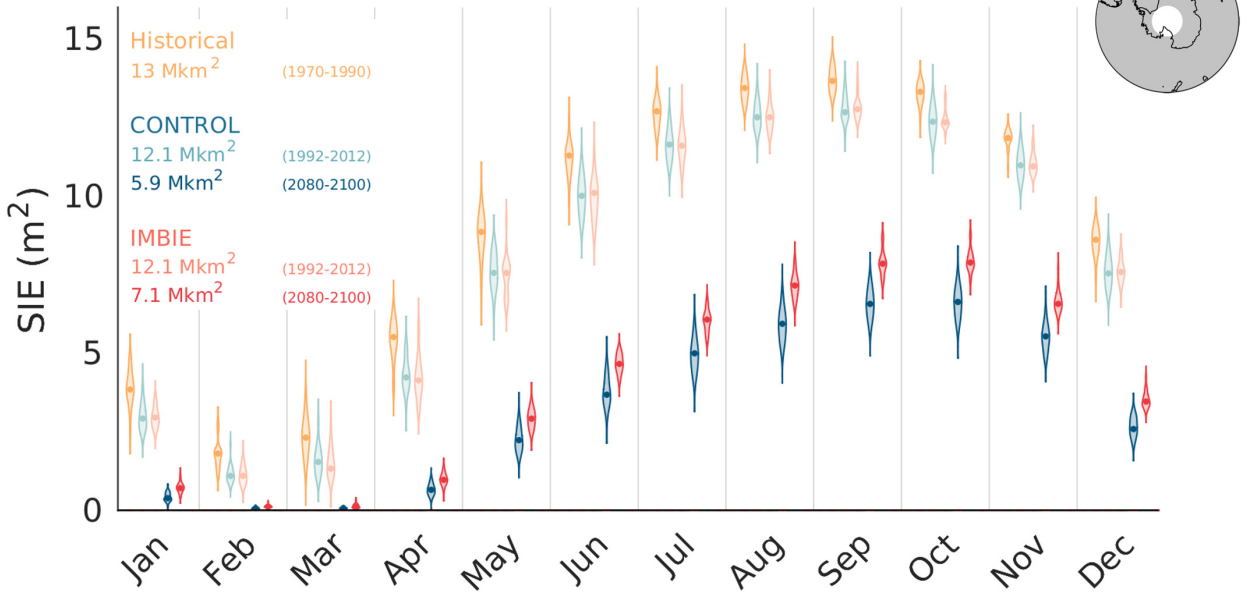


B IMBIE – CONTROL
(2080-2100)



C

Southern Ocean



D

AB Seas

